Journal of Statistical Physics, Vol. 40, Nos. 3/4, 1985

Phase Diagram of the Ising Model on a Cayley Tree in the Presence of Competing Interactions and Magnetic Field

Ananias M. Mariz,[1,2] Constantino Tsallis,[1,2] and E. L. Albuquerque[2]

Received Novmeber 28, 1984; revised March 20, 1985

We study the phase diagram for the Ising Model on a Cayley tree with competing nearest-neighbor interactions J_1 and next-nearest-neighbor interactions J_2 and J_3 in the presence of an external magnetic field. To perform this study, an iterative scheme similar to that appearing in real space renormalization group frameworks is established; it recovers, as particular cases, previous works by Vannimenus and by Inawashiro *et al.* At vanishing temperature, the phase diagram is fully determined, for all values and signs of J_2/J_1 and J_3/J_2; in particular, we verify that values of J_3/J_2 high enough favor the paramagnetic phase. At finite temperatures, several interesting features (evolution of reentrances, separation of the modulated region into two disconnected pieces, etc.) are exhibited for typical values of J_2/J_1 and J_3/J_2.

KEY WORDS: Ising model; Cayley tree; devil's staircase; spin-glass.

1. INTRODUCTION

The Ising model on a Cayley tree with competing interactions has recently been studied extensively because of the appearance of nontrivial magnetic orderings. The Cayley tree is not a realistic lattice; however, its amazing topology makes the *exact* calculation of various quantities possible. It is believed that several among its interesting thermal properties could persist for regular lattices, for which the exact calculation is so far untractable.

Partially supported by the Brazilian Agencies CNPq and FINEP.

[1] Centro Brasileiro de Pesquisas Físicas/CNPq, Rua Dr. Xavier Sigaud, 150, 22290-Rio de Janeiro, RJ—Brazil.

[2] Departamento de Física, Universidade Federal do Rio Grande do Norte, 5900-Natal, RN—Brazil.

0022-4715/85/0800-0577$04.50/0

Furthermore it is equivalent to the standard Bethe–Peierls theory.[1] In particular, considering a system with ferromagnetic nearest-neighbor (nn) interactions and competing (antiferromagnetic) next-nearest-neighbor (nnn) interactions on a Cayley tree, Vannimenus[2] was able to find new modulated phases, in addition to the expected paramagnetic (P) and ferromagnetic (F) ones. These new phases consist in a period-four one (denoted $\langle 2 \rangle$ from now on), and in a complex set of higher-order commensurate or incommensurate modulated phases (denoted M from now

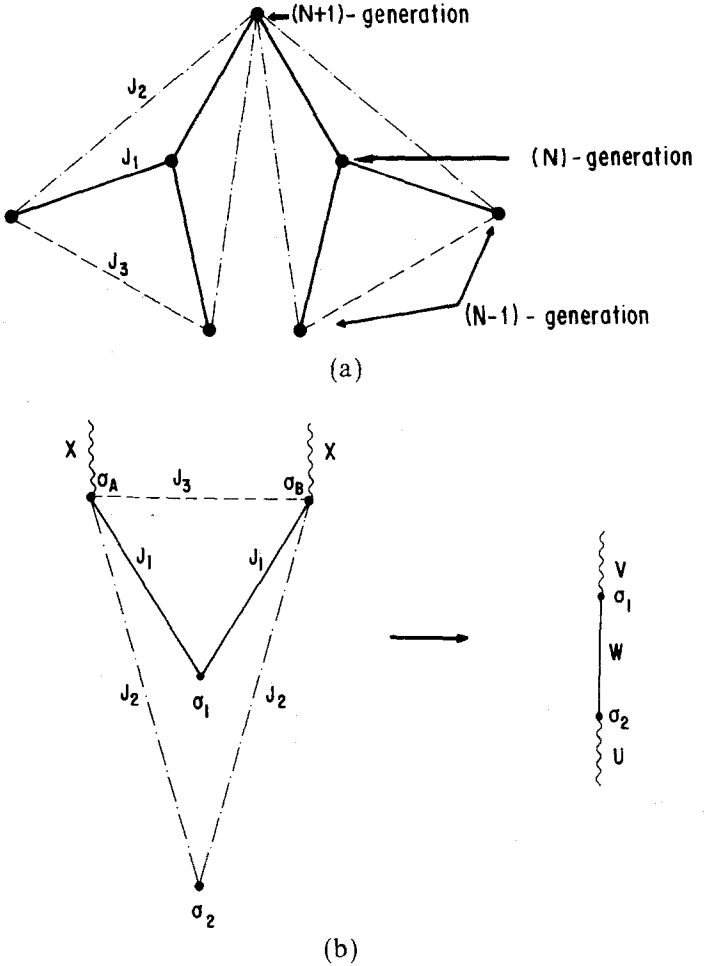

Fig. 1. (a) Three successive generations of a Cayley tree (solid line: nearest-neighbor interactions; dot-dashed line: next-nearest-neighbor interactions; dashed line: interbranch interactions); (b) schematic diagram to illustrate the summation used in Eq. (20).

on). The detailed analysis of the complex M phase has revealed the existence of a "devil's staircase" (similar facts are observed in other models[3-7]). More recently, Inawashiro *et al.*[8,9] investigated the same system on a Cayley tree but, unlike Vannimenus, they included in the model same-generation next-nearest-neighbor interactions; this situation corresponds to the usual Bethe–Peierls approximation on the hexagonal lattice. Using an iteration scheme different from that introduced by Vannimenus, they found similar features. Their detailed analysis of the M phase shows that the local magnetization presents chaotic oscillatory glasslike behavior.

The aim of this paper is to extend in several senses these previous results. First, the presence of an external magnetic field is assumed. Second, our model consists of a spin-1/2 Ising model on a Cayley tree of branching ratio 2 (like Inawashiro *et al.*[9]), where all three interactions are characterized by general strengths (J_1, J_2, $J_3 \gtrless 0$); see Fig. 1a. This model recovers that of Vannimenus for $J_3 = 0$, and that of Inawashiro *et al.* for $J_3 = J_2$. This choice is not a mere mathematical complication of the previous results since, as we shall see later on, a significantly richer phase diagram is obtained. In spite of its simplicity, the branching ratio 2 Cayley tree, already presents several nontrivial effects. These effects should not be very different in higher (but finite) branching ratio trees, excepting for the possible appearance, at *finite* temperatures, of Lifshitz points (see Ref. 6).

The outline of this paper is as follows: in Section 2 we set up the basic equations of our model and we find the recurrence relations. Section 3 is devoted to the analysis of the phase diagram. Finally, the conclusions are presented in Section 4.

2. BASIC EQUATIONS

We consider a Cayley tree with branching ratio 2 (see Fig. 1a). Let us introduce $q \equiv J_3/J_2$ and $p \equiv -J_2/J_1$; obviously for $q = 0$ we recover Vannimenus model, while $q = 1$ is the case focused on by Inawashiro *et al.* In order to set up our basic equations in a recurrence scheme relating the partition function of an N-generation tree to the partition functions of its subsystems, we should take into account the partial partition functions for all the possible configurations of the spins in two successive generations. If we identify (following along the lines of Vannimenus) $Z_N(-^{+}-)$ as the partition function of a branch of an N-generation tree where the spin in the last generation is up and the two spins in the preceding one are down, there are only six different Z_N to consider. We define for convenience the following variables [see Eq. (1) of Ref. 2]: $z_1 \equiv Z_N(+^{+}+)$, $z_2 \equiv Z_N(+^{+}-)$, $z_3 \equiv Z_N(-^{+}-)$, $z_4 \equiv Z_N(+^{-}+)$, $z_5 \equiv Z_N(+^{-}-)$, $z_6 \equiv$

$Z_N(-\bar{\ }-)$, and $u_i \equiv \sqrt{z_i}$ $(i=1, 2,..., 6)$. The effect of the J_3 interaction is appropriately included by a factor $\exp(\pm J_3/k_B T)$ into each Z_i as obtained in Ref. 2; the plus (minus) sign corresponds to the same (opposed) orientation of the two spins of the preceding generation. It is straightforward to establish the following recursive relations:

$$u_1' = a[b^2 c u_1^2 + (2/c)\, u_1 u_3 + (c/b^2)\, u_3^2] \tag{1}$$

$$u_3' = a^{-1}[b^2 c u_4^2 + (2/c)\, u_4 u_6 + (c/b^2)\, u_6^2] \tag{2}$$

$$u_4' = a^{-1}[(c/b^2)\, u_1^2 + (2/c)\, u_1 u_3 + b^2 c u_3^2] \tag{3}$$

$$u_6' = a[(c/b^2)\, u_4^2 + (2/c)\, u_4 u_6 + b^2 c u_6^2] \tag{4}$$

where the prime denotes recurrence image and where the equations for u_2 and u_5 have been omitted as they satisfy $u_2^2 = u_1 u_3$ and $u_5^2 = u_4 u_6$, with

$$a \equiv \exp(J_1/k_B T) \tag{5}$$

$$b \equiv \exp(J_2/k_B T) \tag{6}$$

$$c \equiv \exp(J_3/k_B T) \tag{7}$$

We note that, in the paramagnetic phase (high symmetry phase), $u_1 = u_6$ and $u_3 = u_4$. For discussing the phase diagram, the following choice of reduced variables is convenient:

$$x \equiv (u_3 + u_4)/(u_1 + u_6)$$

$$y_1 \equiv (u_1 - u_6)/(u_1 + u_6)$$

$$y_2 \equiv (u_3 - u_4)/(u_1 + u_6)$$

Equations (1)–(4) yield

$$x' = (a^2 D)^{-1}[b^4(x^2 + y_2^2) + 2(b/c)^2(x + y_1 y_2) + (1 + y_1^2)] \tag{8}$$

$$y_1' = 2D^{-1}[b^4 y_1 + (b/c)^2(y_2 + y_1 x) + y_2 x] \tag{9}$$

$$y_2' = -2(a^2 D)^{-1}[b^4 y_2 x + (b/c)^2(y_2 + y_1 x) + y_1] \tag{10}$$

where

$$D \equiv b^4(1 + y_1^2) + 2(b/c)^2(x + y_1 y_2) + (x^2 + y_2^2) \tag{11}$$

These expressions generalize those obtained in [2] which are recovered for $c = 1$. Furthermore for $b = c$ we recover the equations of Appendix B of Ref. 9.

In order to find the stability limit surface (in the $k_B T/J_1$, p, q space for instance) of the paramagnetic phase, we need to linearize Eqs. (8)–(10) around the fixed point $(x^*, 0, 0)$, since y_1 and y_2 are parameters that vanish in this region (since $u_1 = u_6$ and $u_3 = u_4$). As x' does not depend on y_1 and y_2 in first order, the nontrivial part of the linearization is expressed in terms of the Jacobian

$$\begin{pmatrix} y_1' \\ y_2' \end{pmatrix} = \begin{pmatrix} \lambda_1 & \lambda_2 \\ \lambda_3 & \lambda_4 \end{pmatrix} \begin{pmatrix} y_1 \\ y_2 \end{pmatrix} \tag{12}$$

where

$$\lambda_1 = 2[b^4 + (b/c)^2 x^*]/D_1 \tag{13}$$

$$\lambda_2 = 2[(b/c)^2 + x^*]/D_1 \tag{14}$$

$$\lambda_3 = -2x^*[1 + (b/c)^2 x^*]/D_2 \tag{15}$$

$$\lambda_4 = -2x^*[b^4 x^* + (b/c)^2]/D_2 \tag{16}$$

with

$$D_1 \equiv b^4 + 2(b/c)^2 x^* + x^{*2} \tag{17}$$

$$D_2 \equiv 1 + 2(b/c)^2 x^* + b^4 x^{*2} \tag{18}$$

and

$$x^* = \frac{b^4 x^{*2} + 2(b/c)^2 x^* + 1}{a^2[b^4 + 2(b/c)^2 x^* + x^{*2}]} \tag{19}$$

Two cases should be examined now, according to whether the eigenvalues of (12) are real or complex:

(a) The Para-ferro (Para-antiferro) Transition. When the eigenvalues of (12) are real, the transition line will be characterized by the criterion that the largest (in absolute value), eigenvalue ($\lambda_{\max}$) should be equal to unity. This determines the stability limit surface we were looking for. If the para-ferro (para-antiferro if $J_1 < 0$) phase transition is a second-order one (and it is, as we shall see later on), this surface coincides with the critical surface.

(b) The Para-Modulated Transition. When the eigenvalues of (12) are complex conjugate, the fixed point is approached in an oscillatory way and the stability limit (which coincides with the critical limit for second-order phase transitions) is achieved if we consider the modulus of λ equal to unity. This requirement completely determines the (critical) surface we are looking for.

If an external magnetic field H ($B \equiv H/k_B T$ is a convenient reduced variable) is applied on the system, the corresponding recursive relations can be quite straightforwardly obtained following along the lines of Inawashiro *et al.*[9] The iterative scheme can be set up by summing successively over spins as can be seen in Fig. 1b. We obtain

$$\sum_{\sigma_A, \sigma_B = \pm 1} \exp[K_1(\sigma_1\sigma_A + \sigma_1\sigma_B) + K_2(\sigma_2\sigma_A + \sigma_2\sigma_B) + K_3\sigma_A\sigma_B + X(\sigma_A + \sigma_B)] = C\exp(W\sigma_1\sigma_2 + U\sigma_2 + V\sigma_1) \quad (20)$$

where $K_i \equiv J_i/k_B T$ ($i = 1, 2, 3$) and

$$U \equiv U(X, K_1) = 4^{-1}\ln[\omega(1, 1)\,\omega(1, -1)/\omega(-1, 1)\,\omega(-1, -1)] \quad (21)$$

$$V \equiv V(X, K_1) = 4^{-1}\ln[\omega(1, 1)\,\omega(-1, 1)/\omega(1, -1)\,\omega(-1, -1)] \quad (22)$$

$$W \equiv W(X, K_1) = 4^{-1}\ln[\omega(1, 1), \omega(-1, -1)/\omega(1, -1)\,\omega(-1, 1)] \quad (23)$$

$$C \equiv C(X, K_1) = [\omega(1, 1)\,\omega(1, -1)\,\omega(-1, 1)\,\omega(-1, -1)]^{1/4} \quad (24)$$

with

$$\omega(\sigma, \sigma') = 2e^{K_3}\cosh(2X + 2K_2\sigma + 2K_1\sigma') + 2e^{-K_3} \quad (25)$$

The recursive relations are given by

$$X^{(r)} = B + 2U(X^{(r-2)}, K_1^{(r-2)}) + V(X^{(r-1)}, K_1^{(r-1)}) \quad (26)$$

and

$$K_1^{(r)} = K_1 + W(X^{(r-1)}, K_1^{(r-1)}) \quad (27)$$

for $r = 2, 3, \ldots$ The initial conditions are

$$X^{(0)} = K_1^{(0)} = 0 \quad (28)$$

$$X^{(1)} = B_s \quad (29)$$

$$K_1^{(1)} = K_1 \quad (30)$$

where we have introduced the reduced applied field B_s associated with the outer most shell. B_s need not to be equal to the "bulk" reduced field B, and is introduced for numerical convenience. Indeed, the $B = 0$ phase diagram can only be determined numerically if the up–down symmetry is broken, which is achieved by taking a small value for B_s, for example, $B_s = 0.01$. As a matter of fact, for most regions of the phase diagram, the result does not depend on B_s, which can be chosen to be any arbitrary nonvanishing value; however, regions of the phase diagram might exist for which suf-

ficiently high values of B_s could drive the system to different (high-field) phases (see Refs. 10 and 11 for a discussion of this point for the particular case $J_2 = J_3 = 0$). Equations (21)–(27) recover, for $J_2 = J_3$ and $B = B_s$, those appearing in Ref. 9; furthermore, they lead, for $B = 0$, and through appropriate variable transformations, to Eqs. (8)–(10) of the present paper.

3. THE PHASE DIAGRAM

The recursion relations derived in Section 2 [Eqs. (21)–(30)] provide us the (numerically) exact phase diagram (in the $k_B T/J_1$, p, q, H/J_1 space, for instance) of the problem. Each phase (P, F, M, $\langle 2 \rangle$, AF), is characterized by a particular attractor in the $(X^{(r)}, K_1^{(r)})$ space (note, in particular, that $X^{(r)}$ plays the role of an effective field, thus characterizing the rth shell mean magnetization) and the phase diagram is obtained by following the evolution and detecting the qualitative changements of these attractors. These changements can be either continuous or abrupt, respectively, characterizing second- or first-order phase transitions. A few typical attractors are presented in Fig. 2. In Figs. 3, 4, and 5 we have shown typical critical lines of the vanishing magnetic field phase diagram. It is important to note, first of all, that there is an isomorphism between the system characterized by (J_1, J_2, J_3) and that characterized by $(-J_1, J_2, J_3)$, the main difference being the fact that the ferromagnetic phase corresponds to an antiferromagnetic one. Also the period four modulated phase ($\langle 2 \rangle$) is slightly altered through the isomorphism, changing the order $\uparrow\downarrow\uparrow\downarrow$ by the order $\uparrow\uparrow\downarrow\downarrow$, where the arrows denote four successive shell magnetizations (the different sizes of the arrows refer to different mean values). For the remainder of our analysis we will focus our attention solely on the semiplane $k_B T_c/J_1 \geqslant 0$ since, owing to the isomorphism, we can extend our remarks to the other semiplane $k_B T_c/J_1 < 0$.

The $T = 0$ critical lines of the $J_1 > 0$ phase diagram are particularly simple as they are segments of straight lines (see Fig. 6). The F–$\langle 2 \rangle$ critical line lies along $1/p = 3$, the F–M line along

$$1/p = 3 + q \tag{31}$$

the M–$\langle 2 \rangle$ line along

$$1/p = \begin{cases} 3 - q & \text{if } p \leqslant (2+\sqrt{2})/4 \\ \sqrt{2}(q-1) & \text{if } p \geqslant (2+\sqrt{2})/4 \end{cases} \tag{32}$$

and the P–M line along

$$1/p = q - 1 \tag{33}$$

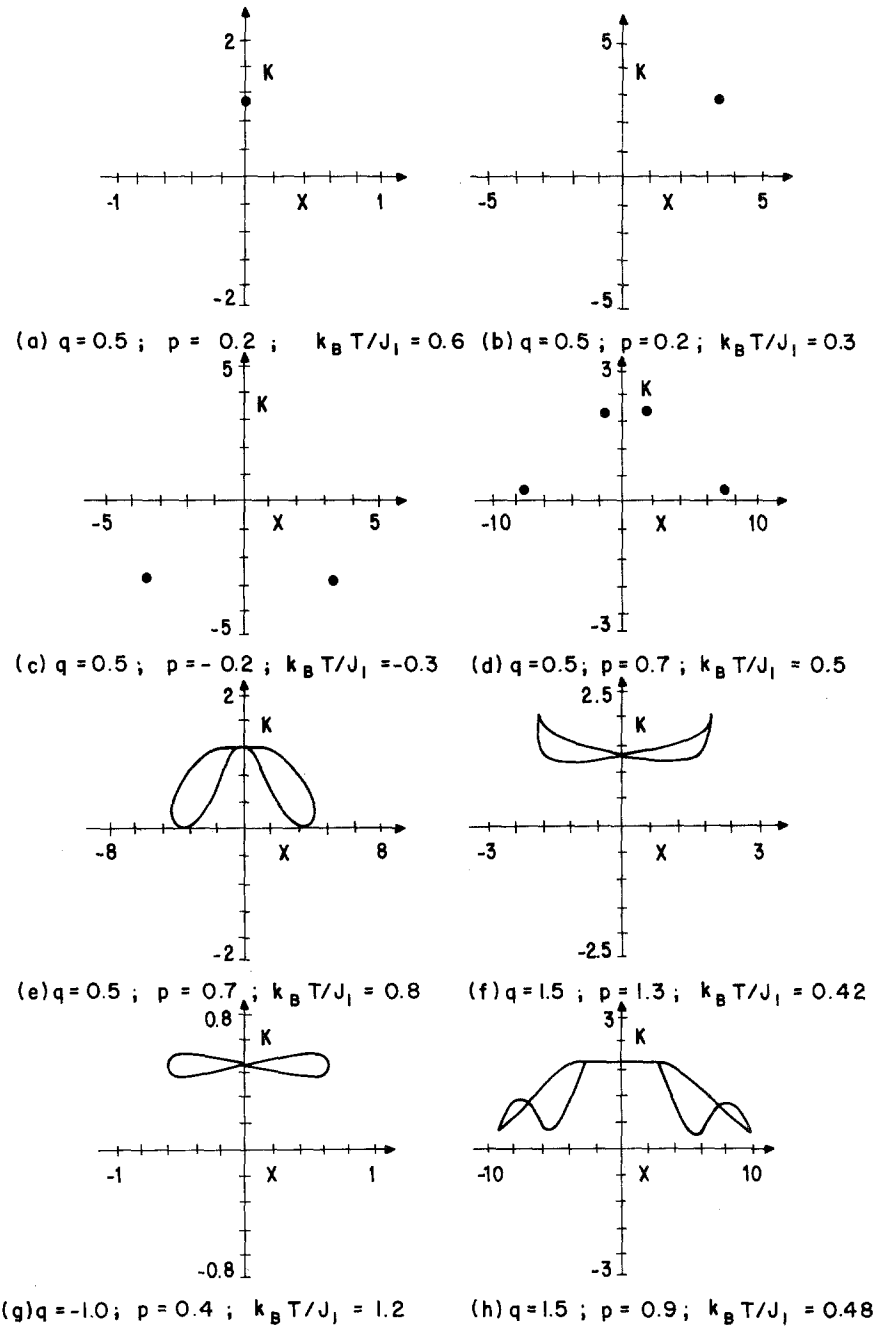

Fig. 2. Examples of attractors in the X–K space [X and K determined by Eqs. (26) and (27)] for vanishing external field and selected values of $q = J_3/J_2$, $p = -J_2/J_1$ and $k_B T/J_1$. They correspond to the following phases: (a) paramagnetic, (b) ferromagnetic, (c) antiferromagnetic, (d) $\langle 2 \rangle$ modulated, (e)–(h) more general modulated phases.

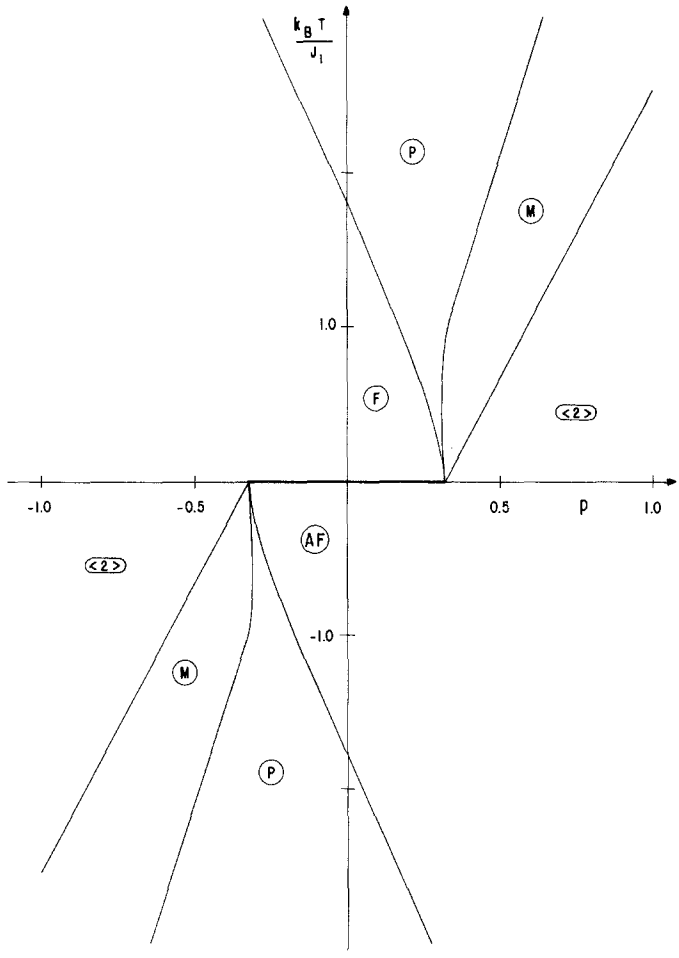

Fig. 3. Phase diagram of the Cayley tree with competing interactions, showing the ferromagnetic (F), antiferromagnetic (AF), paramagnetic (P), modulated (M), and modulated $\langle 2 \rangle$ phases for $q \equiv J_3/J_2 = -1$.

At low temperatures and for $q < 1$, the M phase presents a small reentrance into the paramagnetic phase, as illustrated in Fig. 7. This reentrance becomes more pronounced when q approaches zero from positive values, and decreases again for more and more negative values of q. Another interesting feature is the fact that, for $q > 1$, the $J_1 > 0$ P–M critical temperature attains a *maximum* as a function of p (see Fig. 5), in contrast with the $q \leqslant 1$ cases, where it monotonously increases. Furthermore the M phase appears, for $q = 3/2$, in two *disconnected* pieces (denoted M_1 and M_2; see

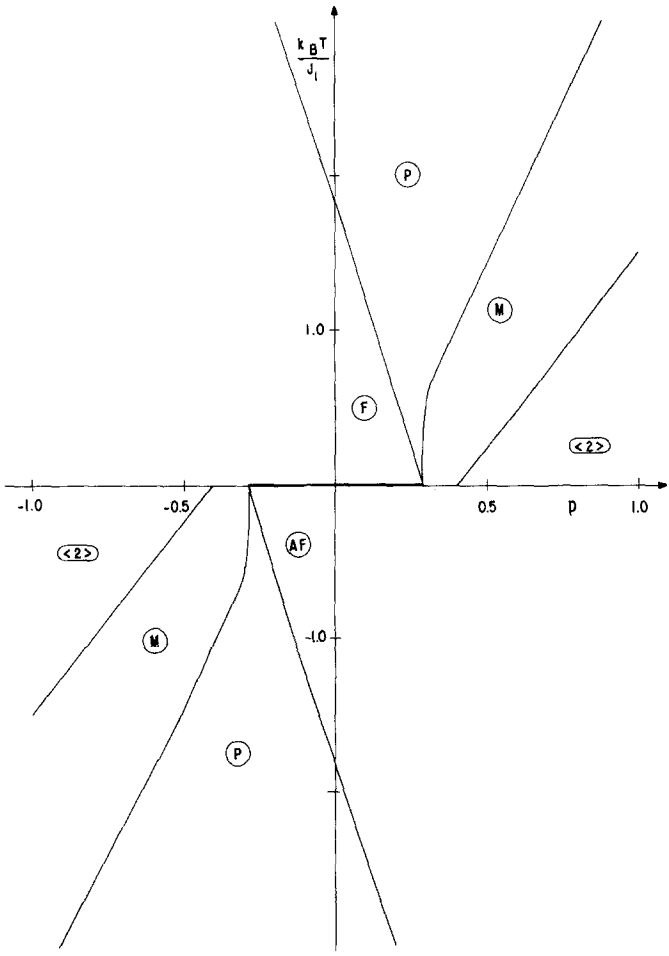

Fig. 4. The same as Fig. 3 but with $q = 0.5$.

Fig. 5), the M_1 and M_2 parts of it being, respectively, associated with attractors of the types indicated in Figs. 2h and 2f. The M_1–$\langle 2 \rangle$ critical line is a second-order one, which is (possibly) not the case for the M_2–$\langle 2 \rangle$ critical line, where the attractor changes *suddenly* (it is of the type Fig. 2d for the $\langle 2 \rangle$ region, and of the type of Fig. 2f for the M_2 region). For $q \gtrsim 3/2$ and $q \lesssim 3/2$, the P–$\langle 2 \rangle - M_1 - M_2$ multicritical point disappears and the two regions M_1 and M_2 become connected through a narrow path (see Fig. 8). An interesting "metastability" phenomenon occurs along this path: there is an intermediate region (shaded in Fig. 8) where during a long transient the attractor seems to be that of region M_2 (i.e., of the type of

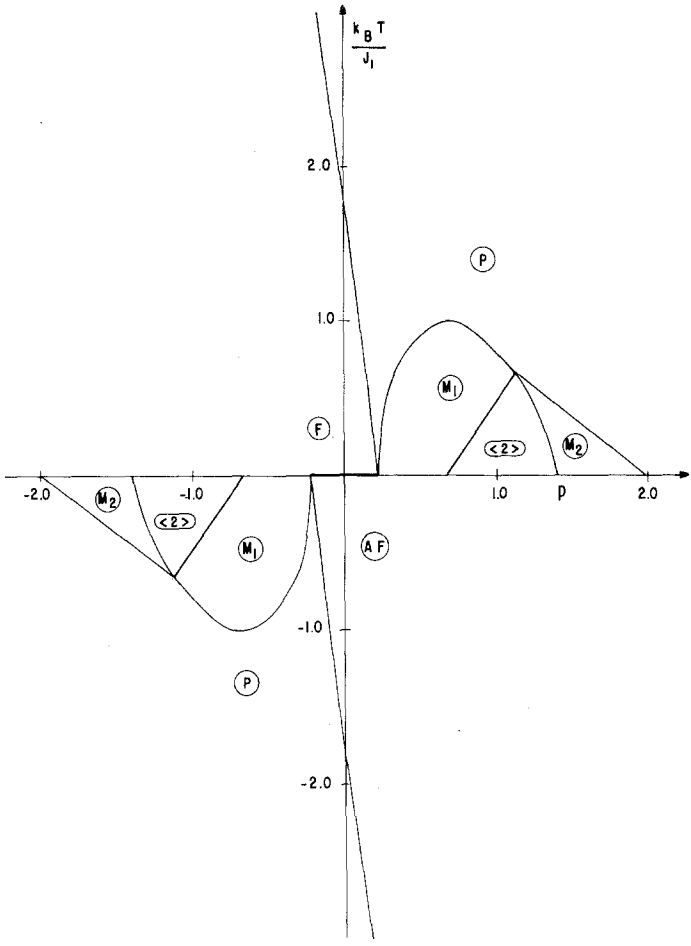

Fig. 5. The same as Fig. 3 but with $q = 1.5$ (the M phase splits into two pieces, denoted M_1 and M_2).

Fig. 2f), but, after many iterations, numerical fluctuations drive the system to its final attractor, namely, that of region $M1$ (i.e., of the type of Fig. 2h). The change of attractor is abrupt and irreversible. This phenomenon means that there is a quite large "surface" region of the Cayley tree where the spin-glass-like ("chaotic" in some sense) magnetic order is quite different from the "bulk" order (which also is spin-glass-like).

If a uniform external magnetic field H is considered, the entire phase diagram will evoluate, excepting of course the F–P critical surface which disappears, the magnetic field H being thermodynamically conjugated of

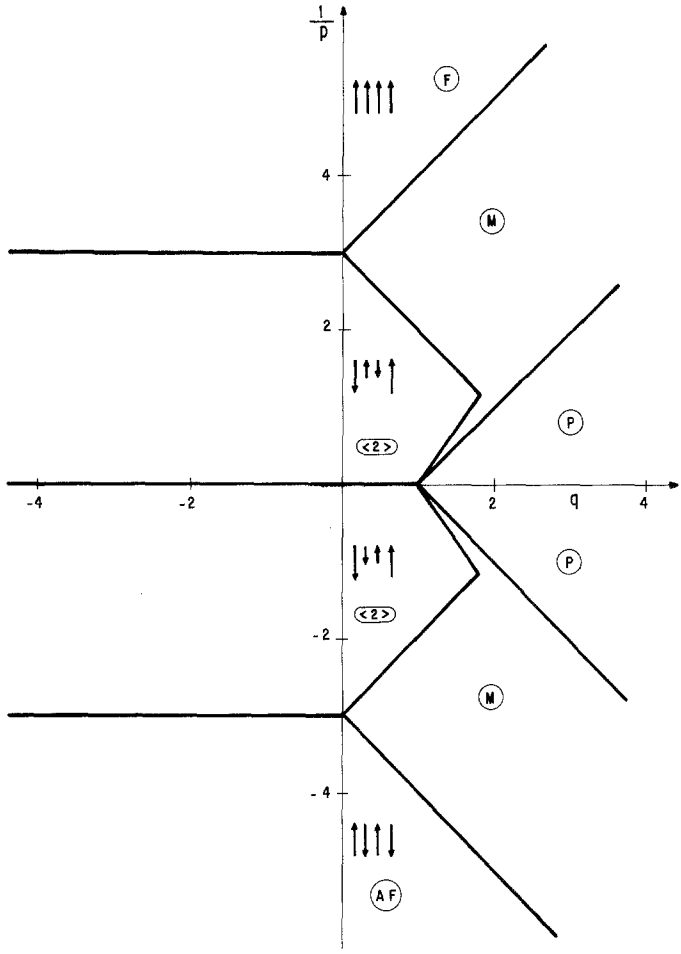

Fig. 6. $T=0$ phase diagram.

the ferromagnetic order parameter (spontaneous magnetization). For the discussion of some aspects of the $J_2=J_3=0$ particular case, see Refs. 12 and 14. The influence of nonvanishing J_2 and J_3 coupling constants has been illustrated in Fig. 9.

4. CONCLUSIONS

In this paper we have extended in several senses previous works by Vannimenus[2] and by Inawashiro *et al.*[8,9] on the Ising model on a Cayley tree with competing interactions. As before, the paramagnetic (P), ferromagnetic (F), period four modulated ($\langle 2 \rangle$), and more complex

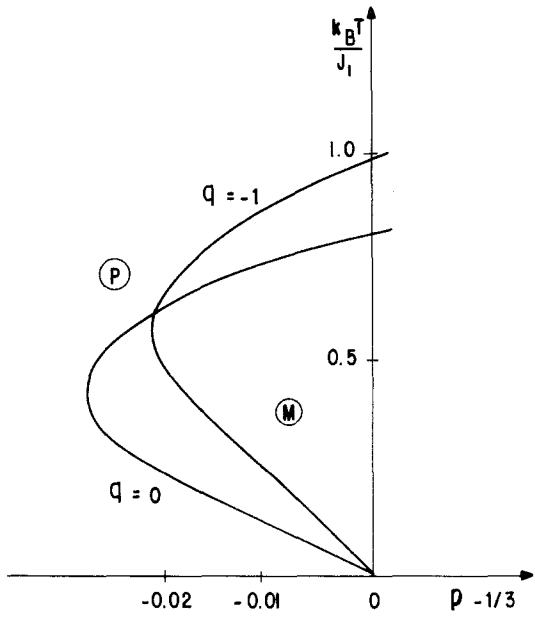

(a)

Fig. 7. Typical reentrances of the modulated phase (M) into the paramagnetic one (P).

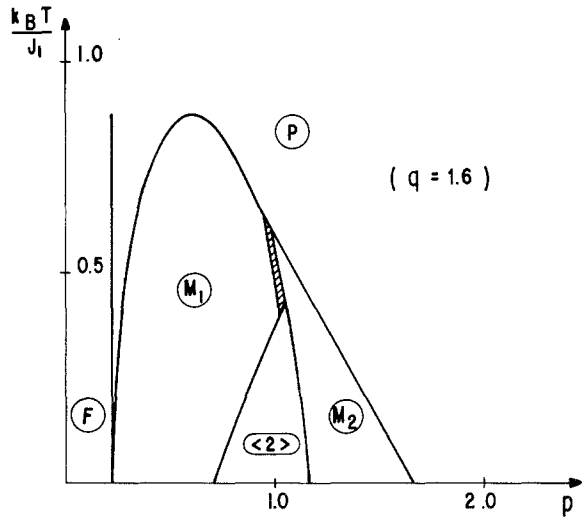

(b)

Fig. 8. Phase diagram for $q = 1.6$. In the shaded region the interesting "metastability" phenomenon described in the text occurs.

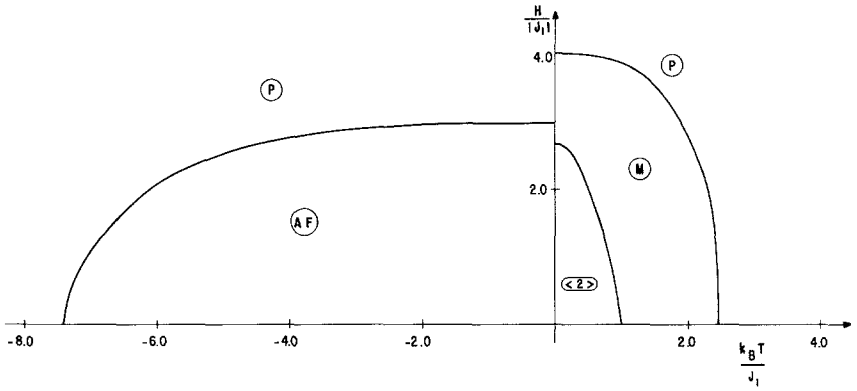

(a)

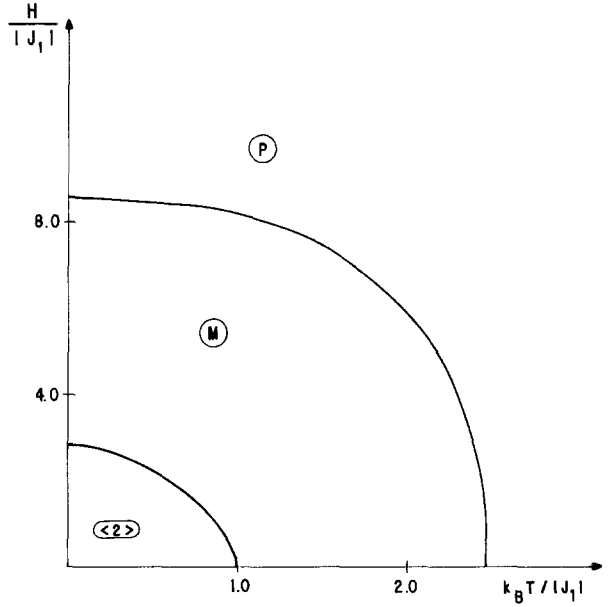

(b)

Fig. 9. Phase diagram in the presence of an external magnetic field H: (a) $p = q = 1$; (b) $p = -q = -1$.

modulated (M) phases are observed, and, through the numerical observation of the various attractors (corresponding to the relevant recurrences), the phase diagram has been determined. Furthermore, we exhibit the vanishing magnetic field ($H=0$) $(J_1, J_2, J_3) \to (-J_1, J_2, J_3)$ isomorphism and show how it is destroyed for $H \neq 0$ (see Fig. 9). Other new features that have been established are the following:

(i) The complete $T=H=0$ phase diagram is made, in the $(1/p, q)$ space ($p \equiv -J_2/J_1$, $q \equiv J_3/J_2$), of pieces of straight lines, and their analytic equations have been established.

(ii) The q-evolution of the small reentrances, in the $(p, k_B T/J_1)$ space, of the M phase into the P phase has been discussed, and it has been verified that the maximal reentrance occurs in the neighborhood of $q=0$.

(iii) The $H=0$, $J_1>0$ P–M critical temperature monotonously increases with p for $q \leqslant 1$, but, for $q>1$, present a *maximum* and then vanishes for p high enough.

(iv) The $H=0$ M–$\langle 2 \rangle$ critical temperature also monotonously increases with p for $q \leqslant 1$ but, for $q>1$, presents a *maximum* and then vanishes for p high enough.

(v) For $q=3/2$, the $H=0$ M–$\langle 2 \rangle$ critical line touches in a (multicritical) point the M–P critical line, in such a way that the $\langle 2 \rangle$ phase separates the M phase into *two disconnected pieces* (noted M_1 and M_2); the attractors associated with each piece are quite different in shape, and naturally they must correspond to quite different "devil's staircases."

(vi) All critical frontiers that have been observed are continuous ones (no latent heat), excepting the M_2–$\langle 2 \rangle$ and M_1–M_2 critical lines in the neighborhood of $q=3/2$; in this case interesting "metastability" phenomena have been exhibited, which essentially means that the "surface" shells (a quite large number of then) of the Cayley tree present a modulated order quite different from that of the "bulk."

The detailed study of the q-evolution (including the metastability effects) of the devil's staircases associated with the modulated phase(s) of the present competing interactions Cayley tree would be very welcome; it could reveal interesting aspects that could exist even for regular lattices, and consequently be of relevance for real spin-glasses. Although the Cayley tree is not a realistic model, we hope that the results obtained in the present work can simulate the behaviour of more realistic systems. As pointed by Vannimenus, a Cayley tree is a counterpart of the ANNNI model, which is used to provide an approximate description of some materials, such as CeSb and ferroelectric $NaNO_2$. Other possible realizations of a system with properties similar to those of the Cayley tree are those where there is a gradient in the density of magnetic atoms, as suggested by Moraal.[10]

ACKNOWLEDGMENTS

We are indebted to S. G. Rosa Jr. for stressing our attention on this problem, and to A. O. Caride for computational assistance. One of us (C.T.) also acknowledges useful remarks from S. R. Salinas, M. J. de Oliveira, S. B. Cavalcanti, J. R. L. de Almeida, and S. G. Coutinho.

REFERENCES

1. S. Katsura and M. Takizawa, *Prog. Theor. Phys.* **51**:82 (1974).
2. J. Vannimenus, *Z. Phys. B* **43**:141 (1981).
3. M. E. Fisher, *Physica* **106A**:28 (1981); W. Selke and P. M. Duxbury, *Z. Phys. B* **57**:49 (1984).
4. P. Bak and J. von Boehm, *Phys. Rev. B* **21**:5297 (1980); N. M. Svrakić, J. Kertész, and W. Selke, *J. Phys. A* **15**:L427 (1982).
5. S. R. McKay, A. Nihat Berker, and S. Kirkpatrick, *Phys. Rev. Lett.* **48**:767 (1982).
6. C. S. O. Yokoi, M. J. de Oliveira, and S. R. Salinas, *Phys. Rev. Lett.* **54**:163 (1985); J. G. M. A. Moreira and S. R. Salinas (unpublished).
7. K. Fesser and H. J. Herrmann, *J. Phys. A* **17**:1493 (1984); C. S. O. Yokoi and M. J. de Oliveira, *J. Phys. A* **18**:L153 (1985).
8. S. Inawashiro and C. J. Thompson, *Phys. Lett.* **97A**:245 (1983).
9. S. Inawashiro, C. J. Thompson, and G. Honda, *J. Stat. Phys.* **33**:419 (1983).
10. H. Moraal, *Physica* **92A**:305 (1978).
11. H. Moraal, *Physica* **105A**:472 (1981).
12. E. Müller-Hartmann and J. Zittartz, *Phys. Rev. Lett.* **33**:893 (1974).
13. E. Müller-Hartmann and J. Zittartz, *Z. Phys. B* **22**:59 (1975).
14. C. E. T. Gonçalves da Silva, *J. Phys. C* **12**:L219 (1979).